ChemComm

Discovery of alkaline-stable nickel manganese oxides with visible photoresponse for solar fuels photoanodes

Journal:	*ChemComm*
Manuscript ID	CC-COM-10-2017-008002.R2
Article Type:	Communication

Journal Name

COMMUNICATION

Alkaline-stable nickel manganese oxides with ideal band gap for solar fuels photoanodes

Santosh K. Suram,[a] Lan Zhou,[a] Aniketa Shinde,[a] Qimin Yan,[bc] Jie Yu,[bc] Mitsutaro Umehara,[ad] Helge S. Stein[a] ,Jeffrey B. Neaton,[c] and John M. Gregoire*[a]

Received 00th January 20xx,
Accepted 00th January 20xx

DOI: 10.1039/x0xx00000x

www.rsc.org/

Abstract: Combinatorial (photo)electrochemical studies of the (Ni-Mn)O_x system reveal a range of promising materials for oxygen evolution photoanodes. X-ray diffraction, quantum efficiency, and optical spectroscopy mapping reveal stable photoactivity of $NiMnO_3$ in alkaline conditions with photocurrent onset commensurate with its 1.9 eV direct band gap. The photoactivity increases upon mixture with 10-60% Ni_6MnO_8 providing an example of enhanced charge separation via heterojunction formation in mixed-phase thin film photoelectrodes. Computational characterization of the band edges reveals the importance of the Hartree-Fock exchange potential in understanding the excellent valence band alignment for water oxidation.

Solar driven electrochemical conversion of H_2O and CO_2 into chemical fuels is a promising approach for generating renewable energy, as chemical fuels offer high energy density and ease of energy storage and distribution. Of the several critical advancements required to realize an efficient photoelectrochemical (PEC) solar fuels technology,[1] the development of an efficient, stable, and earth-abundant oxygen evolution reaction (OER) photoanode poses the most substantial challenge for materials discovery.[2] State-of-the-art device efficiency models, which include practical consequences of using earth-abundant materials, indicate that 15% solar to hydrogen conversion efficiency with a tandem absorber device can only be obtained with a 1.8-2.0 eV band gap for the top absorber, a very tight range that precludes nearly all existing photoanode materials.[2-3] This efficiency-related constraint is combined with the thermodynamic requirement that the conduction band minimum (CBM) and valence band maximum (VBM) of the photoanode must straddle the OER Nernstian potential (1.23 V vs RHE). Furthermore, to attain sufficient photovoltage from the relatively low-gap photoanode, the VBM must be at higher energy (lower electrochemical potential) than traditional photoanode materials whose deep O 2p VBM states correspond to photoelectrochemical potential loss of approximately 1 V.

Devices that operate in extreme pH electrolytes benefit from high catalytic rates and low systems losses, in particular due to the high ion transference in the ion conducting membrane separating the oxygen evolution photoanode from the fuel-forming reaction.[4] While metal oxides comprise a promising class of materials for attaining the desired band gap energy that also resists self-oxidation in the highly oxidizing OER environment, (photo)electrochemical stability at extreme pH remains a daunting task in photoanode development with few materials exhibiting thermodynamic stability under operating conditions.[2] $NiMnO_3$ was recently proposed as such a material with a predicted stability window of pH 7.5 to pH 14 at 1.23 V vs RHE,[5] and in the present work we demonstrate photoanodic activity of $NiMnO_3$ and demonstrate its promise as a photoanode for efficient solar fuels generation.

The presence of Mn in natural photosystems[6] and the demonstration of excellent OER catalytic activity of Ni-based systems[7] has motivated the study of several Ni-Mn-O phases as dark OER catalysts. Photocatalytic systems employing $[Ru(bpy)_3]^{2+}$ and $S_2O_8^{2-}$ as a photosensitizer and a sacrificial electron acceptor, respectively, have utilized Ni-Mn oxides as OER catalysts in near-neutral electrolytes. $NiMnO_3$ catalysts have been shown to improve performance over that of binary Ni and Mn oxides in the pH 7 environment.[8] Ni_6MnO_8 also showed catalytic activity in similar experiments,[9] and OER electrocatalytic activity of several Ni-Mn oxides has been demonstrated in alkaline conditions.[10] In this latter work, nanoporous $NiMnO_3$ exhibited a relatively high overpotential of 0.67 V for 10 mA cm^{-2} in 0.1 M KOH, more than 0.1 V higher than $NiMn_2O_4$, indicating that while $NiMnO_3$ possesses some native catalytic activity for OER, it is not among the best catalysts in alkaline conditions. We recently reported photoactivity in Ni_6MnO_8 thin films with low external quantum efficiency (EQE) on the order of 10^{-5} for oxygen evolution with ultraviolet illuminated.[11] Despite

[a] Joint Center for Artificial Photosynthesis, California Institute of Technology, Pasadena, CA 91125, USA. Email: gregoire@caltech.edu
[b] Department of Physics, Temple University, Philadelphia, PA 19122.
[c] Joint Center for Artificial Photosynthesis, Lawrence Berkeley National Laboratory; Department of Physics, University of California Berkeley; and Kavli Energy NanoSciences Institute, Berkeley, CA 94720, USA.
[d] Future Mobility Research Department, Toyota Research Institute of North America, Ann Arbor MI 48105, USA.

† Electronic Supplementary Information (ESI) available: methods, stability data and additional characterization. See DOI: 10.1039/x0xx00000x

the electrocatalytic investigations of $NiMnO_3$ and theory predictions of its suitability as a photoanode,[5] to the best of our knowledge its photoactivity has not been reported to date.

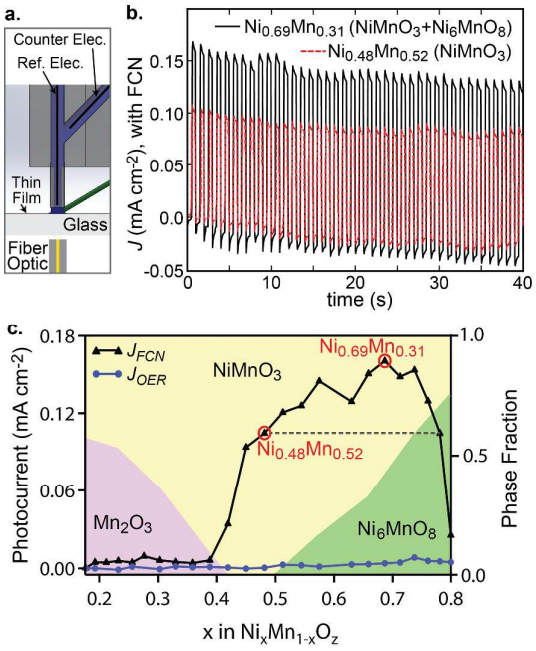

Figure 1. (a) Illustration of the combinatorial PEC cell for the FCN redox couple experiments. (b) Raw chopped-illumination CA measurements for 2 representative samples demonstrating photoanodic activity. (c) Photocurrent density across the $Ni_xMn_{1-x}O_z$ composition spread at OER Nernstian potential (average over the last 3 illumination cycles of the 40 s measurement excluding the transients). The measurements with and without the FCN redox couple are shown with a background color map indicating the composition-dependent phase behavior (right axis). The horizontal dashed line shows the composition interval over which the photoactivity of the phase mixture exceeds that of $NiMnO_3$.

The use of combinatorial sputtering to discover and develop solar fuels photoelectrocatalysts has recently accelerated the materials discovery and development, in particular through the demonstration that off-stoichiometric compounds exhibit unique PEC properties.[12] To assess the photoactivity of $NiMnO_3$, we prepared a $Ni_xMn_{1-x}O_z$ continuous composition spread centered on the target x = 0.5 composition with variation of x by approximately ± 0.3 to explore both off-stoichiometric variants of $NiMnO_3$ and materials in the neighboring phase fields (see Ref. [13] for sputter system details). The thin film composition library (see Figure S1) was synthesized atop a glass substrate with SnO_2:F conducting layer (TEC-7) by reactive co-sputtering of Ni and Mn sources using 83 W and 150 W radio-frequency (RF) power supplies, respectively. The deposition proceeded in mixed O_2 (0.16 Pa) and Ar (0.64 Pa) with 10^{-5} Pa base pressure and was followed by a post-deposition anneal for 10 hours in air at 823 K. The metal oxide compositions were characterized by x-ray fluorescence (XRF) to obtain values of x = Ni / (Ni + Mn) with 10% relative error; the oxygen signal and thus stoichiometry is not detectable by the XRF experiment. The film was further characterized by x-ray diffraction (XRD), confirming the presence of phase-pure $NiMnO_3$ alloys (within the XRD detection limits) over about 10 at.% (x approximately 0.4 to 0.5). In the neighboring phase fields at lower and higher x values, $NiMnO_3$ is mixed with Mn_2O_3 and Ni_6MnO_8, respectively.

To assess the photoanodic performance across the composition library in aqueous pH 13 (0.1 M NaOH) electrolyte, 2 types of toggled-illumination PEC experiments were performed via chronoamperometry (CA) using a scanning drop cell (SDC) coupled to a 385 nm light emitting diode (LED, see Table S1).[14] The ultraviolet LED was chosen to ensure sufficient photoexcitation of any visible band-gap semiconductor, and a schematic of the back-side illumination configuration of the SDC is shown in Figure 1a with example CA measurements shown in Figure 1b. Oxygen evolution photoelectrocatalysis was assessed by using O_2 sparged electrolyte and toggling front-side illumination with the back contact of the composition library biased at 1.23 V vs RHE. As shown in Figure 1c, little photo-response was observed across the composition library with the only measureable photocurrent density (J_{OER}) arising in Ni-rich compositions with values below 0.01 mA cm^{-2}. The poor OER PEC performance prompted an additional experiment in which 0.05 M of both ferri- and ferro-cyanide (FCN) were added to the electrolyte to poise the electrolyte potential at the redox couple equilibrium, approximately 0.1 V below the OER Nernstian potential.[15] Under short circuit conditions, facile 1 e- reduction and oxidation of the FCN redox couple provides screening for photoactivity in the absence of catalytic kinetic barriers, and since the redox potential is similar to the pH 13 OER Nernstian potential, the identification of anodic photocurrent density (J_{FCN}) for a range of thin film compositions (Figure 1b,1c) demonstrates that these photoanodes approximately meet the thermodynamic band alignment requirement for OER photoelectrocatalysis. Mott-Schottky Analysis corroborates the n-type doping of this material and reveals a flatband potential in the vicinity of the photocurrent onset potential, which was determined to be near 1.2 V vs. RHE as shown in Figs. S7 and S10.

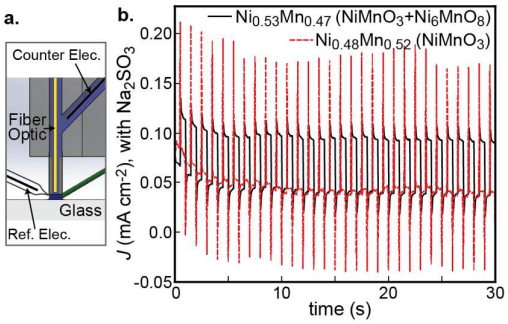

Figure 2. (a) Illustration of the PEC cell for the front-side illumination measurements. (b) Chopped-illumination CA at 1.23 V vs RHE with sodium sulfite hole acceptor for representative samples of the 2 phase fields of interest.

Comparing the compositional variation of J_{FCN} with the phase map reveals the relative inactivity of mixed-phase Mn_2O_3 + $NiMnO_3$ samples. In the phase-pure $NiMnO_3$ region, a sharp rise in J_{FCN} is observed with increasing Ni concentration with the near-stoichiometric $NiMnO_3$ materials showing marked improvement over Mn-rich films. The asymmetric alloying in this Ni^{+2}, Mn^{+4} phase is understandable from the relative ease of Mn to adopt the +2 valence on the Ni site compared to Ni adopting the +4 valence on the Mn site, and the data indicate that Mn^{+2} substitutions are

detrimental to charge separation and/or transport. Since J_{FCN} continues to rise with increasing Ni concentration, the most Ni-rich phase-pure composition ($Ni_{0.48}Mn_{0.52}$) was chosen to represent the $NiMnO_3$ phase. The highest J_{FCN} is observed at the $Ni_{0.69}Mn_{0.31}$ composition where the thin film contains approximately 40% Ni_6MnO_8 phase. Materials with Ni_6MnO_8 concentration in excess of 70% offer no improvement compared to the phase-pure $NiMnO_3$.

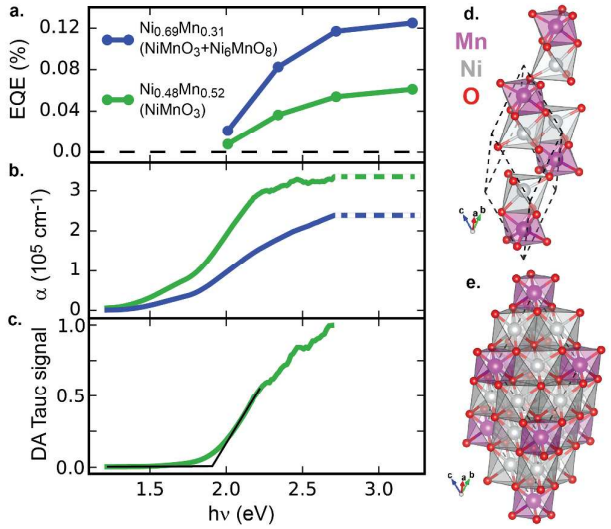

Figure 3. (a) Spectral EQE for the representative samples of $NiMnO_3$ and its mixture with Ni_6MnO_8. (b) Spectral absorption coefficient for the same two samples calculated from optical spectroscopy and XRF-based measurement of film thickness, 195 nm and 220 nm for $Ni_{0.48}Mn_{0.52}$ and $Ni_{0.69}Mn_{0.31}$, respectively. The amount of transmitted light is near the detectability limit of the spectrometer for photon energies above 2.7 eV, leading to excessive noise and prompting the plotting of a dotted line to represent saturation in the α signals at higher photon energies. (c) Direct-allowed Tauc signal calculated from the spectral absorption coefficient with black lines illustrating the identification of a 1.9 eV direct band gap of $NiMnO_3$. Model structures are shown for (d) $NiMnO_3$ and (e) Ni_6MnO_8.

As detailed below, the photoactive $NiMnO_3$ and $NiMnO_3$ + Ni_6MnO_8 thin films in Figure 1 are optically thick at the 385 nm LED wavelength. As a result, the observation of photoactivity with backside illumination indicates that these materials have substantial hole mobility, in agreement with the electronic structure analysis by Yu et al.[5] which notes that Ni d and O p hybridization in the valence band results in large band dispersion along the Γ-Z direction. To ascertain whether back side illumination is a requirement for photoactivity, thin film samples prepared similarly to those in Figure 1, but with approximately 70% of the thickness, were analyzed in a 0.1 M NaOH and 0.1 M Na_2SO_3 electrolyte, the latter being a low-kinetic-barrier hole acceptor. The resulting chopped-illumination CAs at 1.23 V vs RHE are shown in Figure 2. These data indicate that while both $NiMnO_3$ and $NiMnO_3$ + Ni_6MnO_8 samples are photoactive with front-side illumination, the improvement in steady state photocurrent of $NiMnO_3$ upon addition of Ni_6MnO_8 (approximately 12% molar fraction in this sample) is even more drastic than that of Figure 1 (see Figure S4). The $NiMnO_3$ sample exhibits large transients upon illumination toggling that are typically associated with the charging and discharging of surface states.[16] While the presence of the hole acceptor should mitigate these transients, they remain pronounced in this sample, suggesting that even the low barrier to oxidation of sodium sulfite is problematic for the $NiMnO_3$ surface, indicating that this photoanode would greatly benefit from optimized surface chemistry and/or addition of a co-catalyst. The lowered current transients and improved steady state photocurrent upon addition of Ni_6MnO_8 indicates a change in the surface chemistry and/or charge the separation process.

Since the measurements in the presence of the FCN provided the best characterization of the photoactivity of $NiMnO_3$, we return to this technique to characterize its spectral response by measuring J_{FCN} using 4 different illumination sources (610, 530, 455, and 385 nm LEDs) on duplicate samples of those in Figure 1b. By additionally measuring the incident photon flux (see Table S1), the EQE (also referred to as the incident photon to current efficiency) is calculated and shown in Figure 3a. The 2 samples exhibit similar variation of EQE with photon energy, with the phase mixture consistently outperforming the phase-pure sample by a factor of about 2, indicating that the presence of Ni_6MnO_8 enhances charge separation or transport of the $NiMnO_3$ absorber.

Figures 3b-3c show the optical characterization of the samples by combined transmission and total reflection spectroscopy. The Tauc analysis of the $NiMnO_3$ sample indicates a direct-allowed band gap at approximately 1.9 eV, which is commensurate with the onset of photoactivity in Figure 3a. $NiMnO_3$ exhibits a remarkably high absorption coefficient above its 1.9 eV direct band gap, and the onset of photoactivity near this energy indicates that its potential solar to fuel conversion efficiency in a tandem-absorber device is 16%-20% according to the state of the art model, depending on the parameters of other device components.[3] As shown in Figure S2, no detectable degradation in activity was observed when expanding the experiment of Figure 1b to 30 minutes of toggled illumination, indicating that the predicted Pourbaix stability under these conditions extends also to photoelectrochemical stabilty.[5] This level of stability with sub-2 eV band gap is only rivaled by Fe_2O_3[17] and Fe_2WO_6.[18]

The PEC data indicate that the VBM of $NiMnO_3$ is well aligned to the OER Nernstian potential, which implies that the edges of the 1.9 eV band gap straddle the water redox potentials. A previous calculation of the band structure using the screened hybrid functional of Heyd, Scuseria, and Ernzerhof (HSE)[19] with mixing parameter for the Hartree-Fock exchange potential set to 25% is commensurate with this band alignment, but the band gap was found to be approximately 3 eV in that calculation.[5] The band diagram from that work also indicates that $NiMnO_3$ is a pseudo-direct material with the lowest transition being indirect-allowed (Γ-B) with direct-allowed transitions at about 10% higher energy at the Γ, B, XQ, and P points; the existence of direct transitions at several points in the Brillouin zone may give rise to the observed high absorptivity. To explore why this HSE calculation may have overestimated the band gap energy compared to the experiments of Figure 3, band gap and band edge calculations were performed with mixing parameter values spanning 10% to 25%, as shown in Figure 4. The results at approximately 14% are in best agreement with the experimental observations. The mixing parameter impacts

the VBM more than the CBM energy due to the strong hybridization of Ni 3d and O 2p states in the valence band. The contributions from these overlapped orbitals pushes the VBM energy to much higher values than typically observed for metal oxides, with Figure 4 supporting the experimental indications of excellent alignment between the VBM and the OER Nernstian potential.

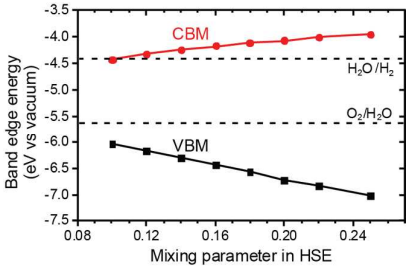

Figure 4. Band edge calculations results from the [001] slab of ferrimagnetic $NiMnO_3$ (6×6×6 supercell) using HSE with various mixing parameters. The water redox potentials are included for reference.

Given the desirable electronic, optical, and stability properties, $NiMnO_3$ merits a concerted effort to improve its radiative efficiency. The high absorptivity corresponds to an extinction depth (1/α) of less than 50 nm for photon energies above about 2 eV, making this material particularly amenable to optimization via nanostructuring. The efficiency-boosting effect of Ni_6MnO_8 also provides avenues for future research. The composition-phase-activity relationships in Figure 1c and the additional data in Figures 2-3 indicate the formation of a straddling-gap or staggered-gap heterojunction between $NiMnO_3$ and Ni_6MnO_8.[20] The measured direct band gap of Ni_6MnO_8 is 2.4 eV and its direct and indirect gaps from HSE calculations with the same 14% mixing parameter noted above are 2.6 and 1.5 eV, respectively, indicating that the $NiMnO_3$ /Ni_6MnO_8 heterojunction is straddling (Type I) with respect to indirect gaps and staggered (Type II) with respect to direct gaps (see Figure S8). Strategies such as a hole blocking layer,[21] thickness and morphology optimization,[22] doping, and improved stoichiometry may be employed to improve the radiative efficiency of $NiMnO_3$-based photoanodes and realize this material's potential for enabling efficient solar fuel generation.

This work is performed by the Joint Center for Artificial Photosynthesis, a DOE Energy Innovation Hub, supported through the Office of Science of the U.S. Department of Energy under Award Number DE-SC000499. The authors thanks Paul F. Newhouse for assistance in optical spectra measurement.

References

1. (a) B. Parkinson, *Accounts of Chemical Research*, 1984, **17**, 431-437; (b) J. Yang, D. Wang, H. Han and C. Li, *Acc Chem Res*, 2013, **46**, 1900-1909; (c) J. R. McKone, N. S. Lewis and H. B. Gray, *Chem Mater*, 2014, **26**, 407-414.
2. K. Sivula and R. van de Krol, *Nature Reviews Materials*, 2016, DOI: 10.1038/natrevmats.2015.10, 15010-15010.
3. K. T. Fountaine, H. J. Lewerenz and H. A. Atwater, *Nat. Comm.*, 2016, **7**, 13706.
4. J. Jin, K. Walczak, M. R. Singh, C. Karp, N. S. Lewis and C. Xiang, *Energ Environ Sci*, 2014, **7**, 3371-3380.
5. J. Yu, Q. Yan, W. Chen, A. Jain, J. B. Neaton and K. A. Persson, *Chemical Communications*, 2015, **51**, 2867-2870.
6. Y. Umena, K. Kawakami, J. R. Shen and N. Kamiya, *Nature*, 2011, **473**, 55-60.
7. (a) R. D. Smith, M. S. Prevot, R. D. Fagan, Z. Zhang, P. A. Sedach, M. K. Siu, S. Trudel and C. P. Berlinguette, *Science*, 2013, **340**, 60-63; (b) J. Yang, K. Walczak, E. Anzenberg, F. M. Toma, G. Yuan, J. Beeman, A. Schwartzberg, Y. Lin, M. Hettick, A. Javey, J. W. Ager, J. Yano, H. Frei and I. D. Sharp, *J Am Chem Soc*, 2014, **136**, 6191-6194; (c) K. Fominykh, J. M. Feckl, J. Sicklinger, M. Döblinger, S. Böcklein, J. Ziegler, L. Peter, J. Rathousky, E.-W. Scheidt, T. Bein and D. Fattakhova-Rohlfing, *Advanced Functional Materials*, 2014, **24**, 3123-3129; (d) C. C. McCrory, S. Jung, J. C. Peters and T. F. Jaramillo, *J Am Chem Soc*, 2013, **135**, 16977-16987.
8. D. Hong, Y. Yamada, A. Nomura and S. Fukuzumi, *Phys Chem Chem Phys*, 2013, **15**, 19125-19128.
9. P. W. Menezes, A. Indra, O. Levy, K. Kailasam, V. Gutkin, J. Pfrommer and M. Driess, *Chem Commun (Camb)*, 2015, **51**, 5005-5008.
10. X. He, F. Yin, Y. Li, H. Wang, J. Chen, Y. Wang and B. Chen, *ACS Applied Materials & Interfaces*, 2016, **8**, 26740-26757.
11. A. Shinde, S. K. Suram, Q. Yan, L. Zhou, A. K. Singh, J. Yu, K. A. Persson, J. B. Neaton and J. M. Gregoire, *ACS Energy Letters*, 2017, DOI: 10.1021/acsenergylett.7b00607, 2307-2312.
12. (a) R. Meyer, K. Sliozberg, C. Khare, W. Schuhmann and A. Ludwig, *ChemSusChem*, 2015, **8**, 1279-1285; (b) K. Sliozberg, H. S. Stein, C. Khare, B. A. Parkinson, A. Ludwig and W. Schuhmann, *ACS Applied Materials & Interfaces*, 2015, **7**, 4883-4889; (c) L. Zhou, Q. Yan, A. Shinde, D. Guevarra, P. F. Newhouse, N. Becerra-Stasiewicz, S. M. Chatman, J. A. Haber, J. B. Neaton and J. M. Gregoire, *Adv. Energy Mater.*, 2015, **5**, 1500968.
13. S. K. Suram, L. Zhou, N. Becerra-Stasiewicz, K. Kan, R. J. R. Jones, B. M. Kendrick and J. M. Gregoire, *Review of Scientific Instruments*, 2015, **86**, 033904-033904.
14. J. M. Gregoire, C. Xiang, X. Liu, M. Marcin and J. Jin, *Rev. Sci. Instrum.*, 2013, **84**, 024102.
15. (a) C. Xiang, J. Haber, M. Marcin, S. Mitrovic, J. Jin and J. M. Gregoire, *ACS Comb. Sci.*, 2014, **16**, 120-127; (b) P. F. Newhouse, D. A. Boyd, A. Shinde, D. Guevarra, L. Zhou, E. Soedarmadji, G. Li, J. B. Neaton and J. M. Gregoire, *J. Mater. Chem. A*, 2016, **4**, 7483-7494.
16. L. M. Peter, *Chemical Reviews*, 1990, **90**, 753-769.
17. K. L. Hardee and A. J. Bard, *Journal of The Electrochemical Society*, 1976, **123**, 1024-1026.
18. M. M. Khader, M. M. Saleh and E. M. El-Naggar, *Journal of Solid State Electrochemistry*, 1998, **2**, 170-175.
19. (a) J. Heyd, G. E. Scuseria and M. Ernzerhof, *Journal of Chemical Physics*, 2006, **124**, 219906; (b) J. Heyd, J. E. Peralta, G. E. Scuseria and R. L. Martin, *Journal of Chemical Physics*, 2005, **123**, 174101.
20. J. Low, J. Yu, M. Jaroniec, S. Wageh and A. A. Al-Ghamdi, *Adv Mater*, 2017, **29**.
21. M. Ma, J. K. Kim, K. Zhang, X. Shi, S. J. Kim, J. H. Moon and J. H. Park, *Chem Mater*, 2014, **26**, 5592-5597.
22. K. J. McDonald and K.-S. Choi, *Energ Environ Sci*, 2012, **5**, 8553-8557.

Table of Contents Entry

Combinatorial photoelectrochemistry combined with first principles calculations demonstrate that $NiMnO_3$ and its mixture with Ni_6MnO_8 are photoanodes with phenomenal absorptivity and band alignment to the oxygen evolution reaction.